Journal of Nuclear Materials 526 (2019) 151747

Contents lists available at ScienceDirect

Journal of Nuclear Materials

journal homepage: www.elsevier.com/locate/jnucmat

Diffusion controlled helium bubble formation resistance of FeCoNiCr high-entropy alloy in the half-melting temperature regime

Da Chen [a], Shijun Zhao [a, b], Jianrong Sun [c, d, **], Pengfei Tai [c, d], Yanbin Sheng [c, d], Yilu Zhao [b], Guma Yeli [b], Weitong Lin [a], Shaofei Liu [a], Wu Kai [e], Ji-Jung Kai [a, b, *]

[a] Department of Mechanical Engineering, City University of Hong Kong, Hong Kong, China
[b] Centre for Advanced Nuclear Safety and Sustainable Development, City University of Hong Kong, Hong Kong, China
[c] Institute of Modern Physics, Chinese Academy of Sciences, Lanzhou, 710000, China
[d] School of Nuclear Science and Technology, University of Chinese Academy of Sciences, Beijing, 100049, China
[e] Institute of Materials Engineering, National Taiwan Ocean University, Keelung, 20224, Taiwan, ROC

HIGHLIGHTS

- FeCoNiCr high-entropy alloy weas irradiated by 2 MeV He^+ in the half-melting temperature regime.
- He bubbles have a smaller size, higher number density, and denser distribution, in high-entropy alloy.
- The helium diffusion through vacancy mechanism was suppressed in high-entropy alloy.

ARTICLE INFO

Article history:
Received 16 April 2019
Received in revised form
30 July 2019
Accepted 7 August 2019
Available online 8 August 2019

Keywords:
High-entropy alloy
Helium bubbles
Point defects behavior
Vacancy concentration
Helium diffusion

ABSTRACT

For the structure materials applied in advanced nuclear energy system, helium bubble formation is always a big concern which will severely degrade the performance of materials around or above the half-melting temperature regime (~0.5 T_m). To explore the He bubble formation resistance in the FeCoNiCr alloy, that is a novel face-centered cubic (fcc) high-entropy alloy (HEA) showing excellent radiation damage tolerance, we conducted a series of 2 MeV He ions irradiation experiments on them at three different temperatures (0.46, 0.51 and 0.57 T_m). For reference purpose, a model *fcc* metallic system of pure Ni was irradiated simultaneously. Through transmission electron microscopy (TEM), He bubble formation in the irradiated samples was systematically investigated. The results show that in any designated temperature, He bubbles have a smaller size, higher number density, and denser distribution in the HEA when comparing to that of pure Ni. The volume fraction of He bubbles is also less in the HEA, suggesting a suppressed bubble evolution. For the underlying mechanism of the He bubble formation resistance of HEA, we suggest that the featured energy barriers for point defects migration in the HEA will promote the recombination of defects and somewhat reduce the vacancy concentration during irradiation. Such unique effect could suppress the He diffusion through vacancy mechanism, it will finally influence the evolution of He bubbles in the HEA.

1. introduction

As a reliable, sustainable and affordable energy, nuclear power has provided about 11% of electricity supply in the world, according to the "World Energy Outlook 2018" released by International Energy Agency (IEA) [1]. Due to its low carbon emission, nuclear energy will play a more critical role in the future energy system [2]. To further increase the energy efficiency and reduce the waste generation, several concepts of Generation IV nuclear power systems have been proposed at the beginning of this century [3]. In contrast to the current reactors, Generation IV nuclear systems are usually designed to operate at higher temperatures and suffer greater radiation damage. It means a harsher service environment for the structure material in them [4]. In addition, more extensive He production

* Corresponding author. Department of Mechanical Engineering, City University of Hong Kong, Hong Kong, China.
** Corresponding author. Institute of Modern Physics, Chinese Academy of Sciences, Lanzhou, 710000, China.
E-mail addresses: sunjr@impcas.ac.cn (J. Sun), jijkai@cityu.edu.hk (J.-J. Kai).

https://doi.org/10.1016/j.jnucmat.2019.151747
0022-3115/

from the transmutation reaction is another issue for the materials applied in the fast neutron reactors [5]. It has known that at the half melting temperature or above it, He bubble will significantly form along grain boundary when the mechanical stress is applied. The growth and coalescence of cavities in the grain boundary can finally lead to the rupture of materials, named as the He embrittlement [6]. In such a background, developing the new structural materials which can stand extreme environment has been a great challenge for the application of advanced nuclear energy.

High-entropy alloys (HEAs), as a new class of metallic material composing with four or more principal elements in equal-molar or near equal-molar constituents [7], have drawn great attention of material scientists in recent years. Due to its excellent mechanical property [8,9], great corrosion resistance [10], strong oxidation resistance [11,12], and promising radiation damage tolerance [13–21], HEAs have also been proposed as one of the candidates for the structural materials of advanced nuclear systems. Till date, the radiation effects of HEAs have been investigated using the ion irradiation by several academics. Kumar et al. found that [14], at the irradiation temperature of 400 °C–700 °C, no void was observed in the fcc Fe–Ni–Mn–Cr HEA up to the ~10 dpa, while the formed dislocation loops have a much smaller size comparing to the conventional Fe–Cr–Ni austenitic alloy. Lu et al. also found that [15], the evolution of radiation-induced defects could also be significantly suppressed through increasing the compositional complexity of single-phase concentrated solid-solution alloys. According to their report, the void formation resistance was improved in the multi-component alloy systems, and the dislocation loop transformation and the radiation-induced segregation (RIS) were suppressed in them. Also, Yang et al. [19] found that the specified alloying elements affect the radiation response of HEAs, e.g., the NiCoFeCrPd has a smaller void swelling than that of NiCoFeCrMn. For the underlying mechanisms of the HEAs' radiation tolerance, Zhang et al. [17] performed the *ab initio* calculations and physical property measurements on the multi-component alloy system; they found that the chemical complexity will cause a substantial reduction in electron mean free path, that will result in a slow energy dissipation process. Moreover, some studies [22,23] using the Density Functional Theory (DFT) suggest that the featured migration behavior of point defects in the HEA will promote the defects recombination and result in a less defect accumulation.

Regarding the He behavior in the HEAs, Chen et al. [24] first investigate the He accumulation and bubble formation in the FeCoNiCr alloy system. They found that at the low irradiation temperatures of 0.3–0.4 T_m, the He accumulation was suppressed in the HEA, that only ~50% of diffused He will form the bubble structure in the 673 K. Also, Yan et al. [25] comparatively studied the He bubble behavior in the Ni and FeCoNiCr HEA and found that the coarsening of He bubble is much slower in the HEA during the post-irradiation annealing. Different from our previous report [24], this work was conducted to investigate the He bubble formation resistance of FeCoNiCr HEA in the half-melting temperature regime. It was irradiated by 2 MeV He^+ at the three elevated temperatures of 773 K, 873 K, and 973 K, which are corresponding to the 0.46, 0.51 and 0.57 T_m (T_m: melting temperature of FeCoNiCr is 1695 K [26]), respectively. A model *fcc* metallic system of Pure Ni was also irradiated simultaneously for reference study, the homologous irradiation temperatures for Ni (T_m: 1728 K) are ~ 0.45 T_m, ~0.51 T_m, and ~0.56 T_m, which are very close to the HEA's. Post irradiation, He bubble distributions in the irradiated samples were systematically characterized by the transmission electron microscopy (TEM). We found that at this temperature range, the featured point defects behavior of HEA will cause the sluggish He diffusion through vacancy mechanism. The effect could suppress the He bubble growth according to the Trinkaus' theory [27].

2. Experimental

2.1. Materials

The quaternary HEA with equal-molar ratio composition was prepared by the arc melting Fe, Co, Ni, Cr with high purity (>99.9%) in an argon atmosphere. After repeatedly melting five times, the ingot was drop-casted into a copper mold to make a slab with a dimension of 5 mm × 5 mm × 1 mm. Then the slab was homogenized at 1373 K for 5 h, followed by water quenching. The pure Ni was treated with the same procedure. Before irradiation, the materials were cut and ground through 1200-grit SiC paper, chemical-mechanical polishing using 20 nm colloidal silica suspension were performed to get a mirror-like surface.

2.2. Ion irradiation

2 MeV He^+ irradiation experiments were performed on the material terminal of Low Energy Heavy Ion Accelerator Facility (LEAF) in Institute of Modern Physics, Chinese Academy of Sciences (IMP, CAS), Lanzhou, China. The samples were irradiated to a fluence of 1.52×10^{20} ions/m^2 at 773 K, 873 K, and 973 K, respectively. During irradiation, He^+ beam flux was controlled at ~4.37×10^{16} ions/m^{2}s, the temperature was well controlled within the error of ±5 K, and vacuum in the irradiation chamber was maintained below 5.0×10^{-5} Pa. A raster beam was used with scanning frequencies of 200 Hz for the horizontal and vertical direction. The stopping and range of ions in matter program (SRIM-2010) [28] were applied to predict the irradiation damage and He concentration along ions incident direction, the quick Kinchin-Pease mode was adopted in this simulation according to suggestions from Stoller et at. [29], the displacement energy was set as 40 eV for all target elements. The ion irradiation conditions are listed in Table 1.

2.3. TEM characterization

Post irradiation, Cross-sectional TEM thin films were prepared by the focused ion beam (FIB) of FEI Scios Dual Beam system, using the standard lift-out method [30]. To remove the artificial damage induced by Ga^+ during FIB milling, the TEM lamellae were further cleaned by Gatan Model 695 Precision Ion Polishing System (PIPS II Pro) at 500 V for 60 s. Following TEM experiments were performed by a JEM-2100F (JEOL) operated at 200 keV, He bubbles were characterized using the through-focus method, which is based on the Fresnel contrast mechanism. For quantitatively analyzing the He bubbles number density in Ni and HEA, the thickness of TEM lamellae were measured from the two-beam convergent beam electron diffraction (CBED) patterns [31], which were acquired in the peak region. The thickness of TEM samples in this study varied from 80–120 nm.

3. Results

The pristine microstructure of the annealed single phase FeCoNiCr HEA has been reported previously. Its average grain size could reach ~420 μm [24], the grain size of pure Ni is larger. It should be

Table 1
Ion irradiation conditions.

Irradiation	2 MeV He^+ with a fluence of 1.52×10^{20} ions/m^2		
Temperature (K)	773	873	973
Nominal peak He concentration (appm)	6831		
Time consumed (s)	~3480		

noted that the following study on He bubble formation were all conducted within the grain, and the boundary effects are neglected due to very limited He penetration depth comparing to the grain size. The radiation damage in displacement per atom (dpa) and He concentration were calculated using SRIM as a function of irradiation depth, showing in Fig. 1. The profiles are overlapping with a low-magnification TEM image acquired from the HEA sample irradiated at 973 K. Obviously, a damaged band showing dark contrast is laying in the depth of ranging from 3.2−3.5 μm.

Fig. 2 is a demonstration for He bubble characterization in the HEA sample irradiated at 973 K. The TEM image of Fig. 2 (a) roughly covering the peak damage region, shows that nanoscale He bubbles locally distribute within a band region with ~400 nm width, below or beyond this range fewer bubble was found. When the TEM film was away from zone axis, Fresnel contrast could be enhanced as shown in the Fig. 2 (b), (d), where the He bubbles are well observed as white and black features in under-focused and over-focused conditions, respectively. It is noted that the observed He bubbles have a relatively uniform size and random spatial distribution, which hinting a homogeneous process for bubble evolution. Generally, the dislocation or interface structure can act as the traps for preferential He bubble nucleation, which will result in a heterogenous bubble formation [6]. In this study, the He + irradiated Ni and HEA all have a single phase fcc structure in the annealing state, which can be seen a homogeneous microstructure for bubble nucleation.

To readily compare the He bubble distribution in the Ni and HEA at different temperatures, a series of cross-sectional TEM images are showing in Fig. 3, which were recorded in the same depth range from 2.8 μm to 3.8 μm at the same scale bar. Excessive defocus value was applied in these images to enhance the contrast of nanosized bubbles. We can find that with increasing irradiation temperature, He bubbles have a broader distribution for both materials. Whereas in any temperature, He bubbles have a narrower distribution band in the HEA. To quantify the He bubble distribution in them, we conducted a statistical analysis on the bubble number density along the depth direction. The results are depicted in Fig. 4, where the data points were obtained in a bin value of ~100 nm. Because of the extremely low number density of bubbles (~$10^{21}/m^3$) beyond the peak region, the scale bar was not included in this analysis. Obviously, He bubbles comply with a similar Gaussian distribution along the ion incident direction, where their peak region of He bubbles all appear in the depth of 3.3−3.4 μm. These distribution curves become flat when the irradiation temperature is increasing. Furthermore, the curves of HEA have a larger gradient, and no He bubbles was detected in the depth range of 2.8−3 μm and 3.6−3.8 μm.

Fig. 5 comparatively displays the He bubbles in the peak region of Ni and HEA. All the TEM images were taken with the same

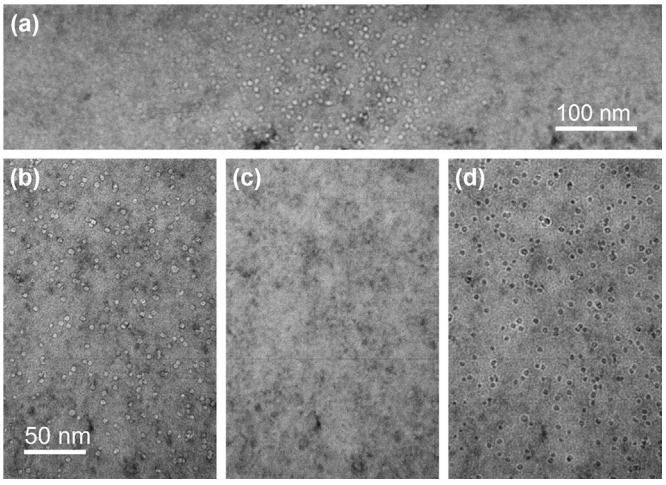

Fig. 2. Demonstration for He bubble investigation through TEM images. (a) a TEM image for 2 MeV He^+ irradiated FeCoNiCr HEA at 973 K, which was acquired in the peak damage/He-concentration region. (b), (c) an (d) are the under-, in- and over-focus TEM images for He bubbles characterization in same position.

defocus value of ~600 nm. It can be found that with increasing temperature, bubble size in both materials become larger while their number density decrease. Meanwhile, He bubbles in the HEA have a smaller size and higher number density comparing to that of Ni case in any specified temperature. In Fig. 6, the average bubble size and number density in the two systems were analyzed. To guarantee the statistical significance, the number density was manually counted from 5 different locations with an area of 100 × 100 nm. The average bubble size was obtained from at least 100 bubbles. The results show that the absolute discrepancy of bubble size between Ni and HEA is slightly larger at a higher temperature. In Table 2, the volume fractions of He bubbles in the peak region were calculated as the ratio of the volume of observed voids to the total sample volume.

4. Discussions

The experimental results show that He bubbles in the HEA have a smaller size, higher number density, denser distribution, as well as a less volume fraction, comparing to the Ni case. It indicates that the HEA has a stronger He bubble formation resistance than that of Ni. Generally, He accumulation and bubble formation in metals are controlled by the He diffusion, which is affected by the irradiation conditions, such as temperature, damage rate, He production rate [6,32]. In order to elucidate the different He bubble behavior in Ni and HEA, we evaluated the effects of point defects behavior on the

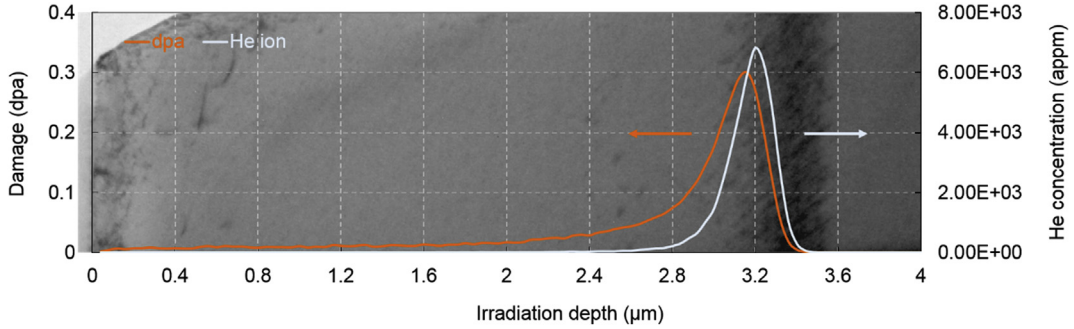

Fig. 1. SRIM calculated ion radiation damage and incident He concentration profiles, overlapping with a cross-sectional TEM image.

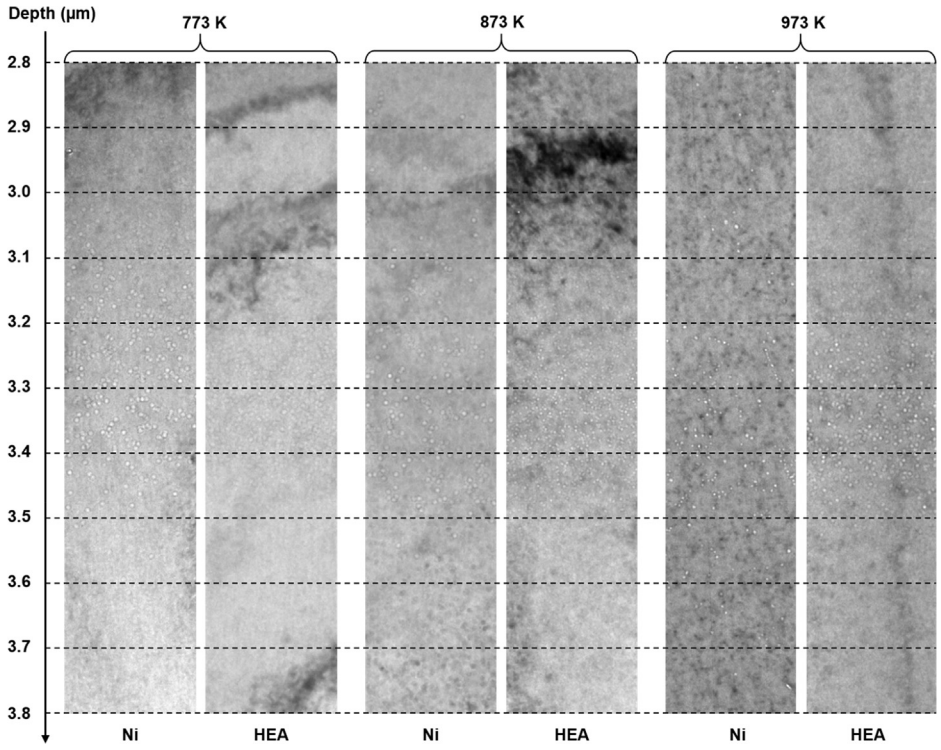

Fig. 3. A series of cross-sectional TEM images for He bubble distribution in pure Ni and FeCoNiCr HEA, which were irradiated by 2 MeV He^+ at 773 K, 873 K and 973 K, respectively. All the TEM images were acquired and cropped from the irradiation depth of 2.8 μm ~3.8 μm.

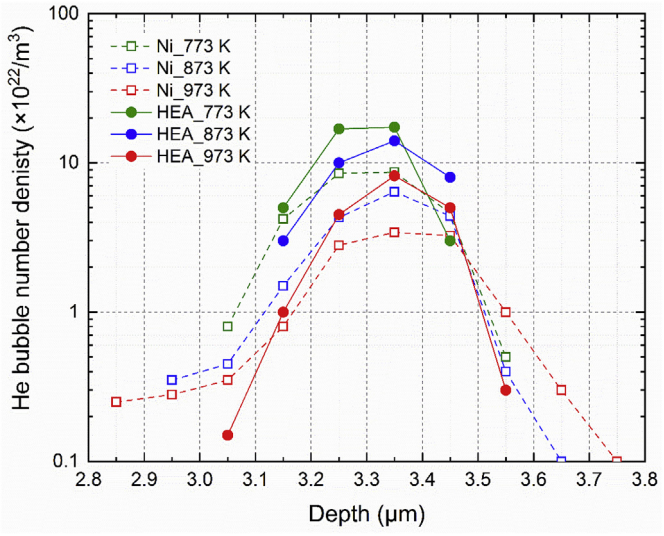

Fig. 4. Statistics for He bubble number density along the irradiation depth from 2.8 μm ~3.8 μm.

He diffusivities in the two metallic systems, then its influence on the He bubble nucleation and growth were figured out.

4.1. Point defects behavior in Ni and HEA

In the He^+ irradiation at elevated temperature, He production is always accompanied by the events of displacement damage, that will concurrently create a lot of *Frenkel* pair defects (vacancy and interstitial) [33]. Since the limited solubility of He in metallic system, the implanted He atoms will diffuse and bonding with vacancies to form bubbles, in turn, the point defect behaviors including its mobility and concentration will have a significant influence on the He behavior, as well as the bubble formation. In Table 3, the energetics of point defects in Ni and HEA were surveyed and summarized according to the *ab initio* calculation by Zhao et al. [22,23], who have performed a systematical study on the defect behavior in the multi-component alloy system. They suggested that the HEA's chemical disorder will lead to the distributions of energy barriers for the point defects, and the overlap of interstitial and vacancy migration energies will promote the defects recombination in HEA [22]. Moreover, we can find that the arithmetic averaged value for interstitial migration energy is larger in HEA, but its vacancy migration energy has a smaller value. It has known that the interstitial usually has a larger diffusivity comparing to the vacancy [33]. If considering the same fcc structure and the similar lattice constant of the two metallic systems, we can qualitatively compare their point defect diffusivities in terms of their migration energies. The lower vacancy migration energy and higher interstitial migration energy in HEA will reduce the difference of their mobility, in contrast to the Ni. It means that the mutual recombination of point defects would be locally enhanced in HEA so that its vacancy concentration caused by the displacement damage will be less than that of Ni. Besides, with increasing the irradiation temperature, thermal vacancy concentration will increase so that the effect of vacancy supersaturation caused by irradiation effects will decline relatively. Thus, the higher vacancy formation energy of HEA showing in Table 3 will result in a lower vacancy concentration, and this effect will be pronounced at a higher temperature. Overall, the featured energetics of point defects in the HEA will intensify the interaction of defects and further lower its vacancy concentration during high-temperature irradiation.

4.2. He diffusion behavior in the irradiated Ni and HEA

From the atomistic perspective, the DFT calculation has

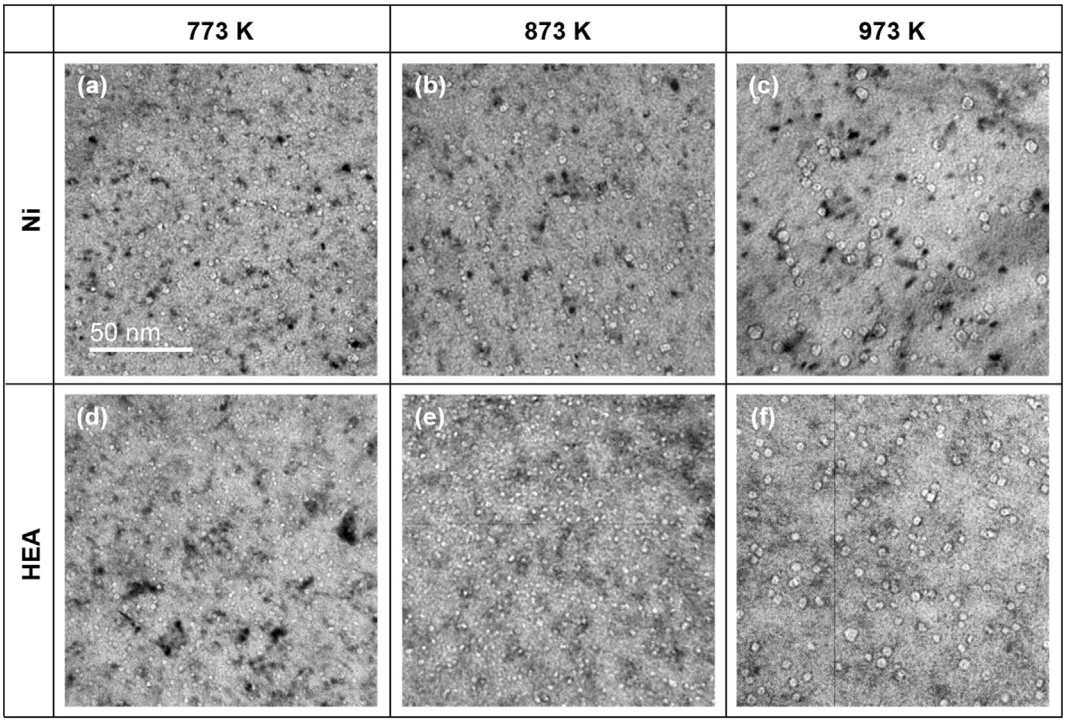

Fig. 5. Comparison of He bubbles in the peak region of pure Ni and FeCoNiCr HEA. (a), (b), (c) are for pure Ni samples at 773 K, 873 K and 973 K, and (d), (e), (f) are for FeCoNiCr HEA samples, respectively. All the TEM images were acquired in the same defocus value.

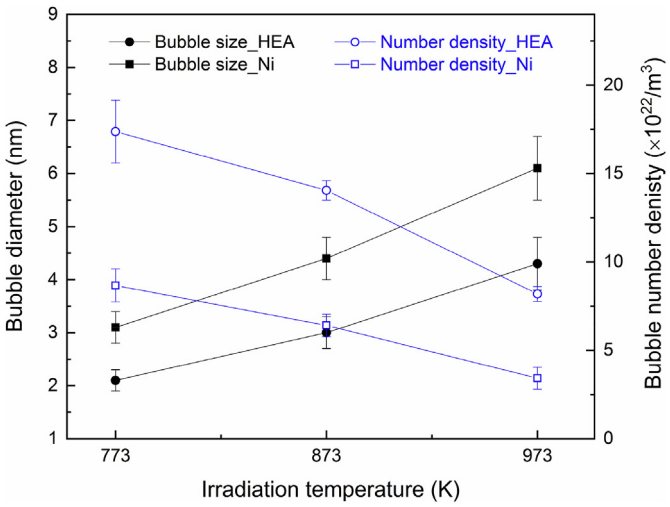

Fig. 6. The size and number density of He bubbles in the pure Ni and FeCoNiCr HEA, which were irradiated by 2 MeV He^+ at 773 K, 873 K, and 973 K.

Table 2
The volume fraction (%) of He bubbles in the peak He region of Ni and HEA.

	773 K	873 K	973 K
Pure Ni	0.03	0.07	0.10
FeCoNiCr HEA	0.02	0.05	0.08

suggested a higher energy barrier for He migration in the HEA either by interstitial or substitutional mode [23], hinting a suppressed He mobility compared to pure Ni. However, He diffusion in the practical situation would be very complicated and profoundly affected by the irradiation conditions. H. Trinkaus proposed that [6], the He diffusion in metals mainly proceeds by three modes of the interstitial migration, the vacancy migration, and the dissociation mechanism by the thermal activation or some athermal displacement. In our situation where a considerable radiation damage rate of ~10^{-4} dpa/s (peak position) exposed around half-melting temperature, the vacancy concentration caused by the irradiation and thermal effect will be very significant. Hence the radiation enhanced vacancy mechanism is believed to dominate the He diffusion process. In such way, the effective He diffusivity could be expressed as [33]:

$$D_{He}^{eff} = C_V * D_V \tag{1}$$

where C_V is the vacancy concentration and D_V is the vacancy diffusivity. For simplicity, we shall first consider the scenario of thermal equilibrium, in which the formula of (3) could be convert to:

$$D_{He}^{eff} = D_0 \exp\left(E_V^F + E_V^M\right) \tag{2}$$

Where D_0 is the pre-factor and can be seen as identical in our systems as above stated. According to the values provided in the Table 3, the increased E_V^F of HEA will overwhelm the decreasing amplitude of E_V^M, so that the activation energy of $E_V^F + E_V^M$ for He diffusion will be higher in HEA, indicating a lower He diffusivity. Aforementioned analysis has shown that the reduced difference of energy barriers for interstitial and vacancy will somewhat enhance the defects recombination in HEA, its higher vacancy formation energy could also result in a lower thermal vacancy concentration. Accordingly, the total vacancy concentration during irradiation is expected to be much lower in the HEA, the decrement would enhanced in the vacancy supersaturation situation like our case. Therefore, we can conclude that the He diffusion through the radiation enhanced vacancy mechanism would be slower in the HEA

Table 3
The energetics of point defects in the He + irradiated Ni and HEA [22,23]. $E_m(V)$ is the migration of vacancy, $E_m(I)$ is the migration energy of interstitial, $E_m^i(He)$ is the He migration energy through interstitial diffusion, $E_m^s(He)$ is the He migration energy through substitutional diffusion, $E_f(V)$ is the vacancy formation energy. For the HEA, the range is given and arithmetic averaged values are provided in parentheses for reference.

	$E_m(V)$	$E_m(I)$	$E_m^i(He)$	$E_m^s(He)$	$E_f(V)$
Pure Ni	1.04	0.15	0.15	1.21	1.45
FeCoNiCr HEA	0.31–1.36 (0.83)	0.00–0.69 (0.31)	0.00–0.80 (0.38)	0.86–1.57 (1.29)	1.58–2.20 (1.83)

comparing to the Ni. Importantly, our statement on He diffusion behavior could also get some clues from our TEM observation on the He bubble distribution. It is well known that implanted ions usually have a Gaussian distribution along the incident direction, and it will broaden at the elevated temperature due to the diffusion effect. In our case, He bubbles in the Ni distribute in a wider region when comparing at the same irradiation condition, it implies that the He could rapidly transport far away from the peak region and promote the He bubble formation there. Therefore, we suggest that the He diffusivity in the HEA is expected to be smaller than that of Ni.

4.3. He bubble formation resistance of FeCoNiCr HEA

In order to interpret the temperature dependence of He bubble formation and further bridge the gap between He diffusivity and the characters of He bubble formation, Trinkaus modeled the evolution of He bubble as the two limiting cases using the kinetic rate equations and classical nucleation theory [34,35]. According to the models, the di-atomic nucleation will dominate the He bubble evolution at low temperature and/or high He production rate conditions, in which the He bubble number density (C_B) and bubble size ($\overline{r_B}$ of the average bubble radius) will comply with the following asymptotic behavior [35]:

$$C_B \propto \left[\left(D_{He}^{eff}\right)^{-\beta} P_{He}^{2(\beta-\alpha)} t^{\beta-\alpha}\right]^{1/(3\beta-2\alpha)} \tag{3}$$

$$\overline{r_B} \propto \left(D_{He}^{eff} P_{He} t^2\right)^{1/(3\beta-2\alpha)} \tag{4}$$

where D_{He}^{eff} is the effective He diffusivity, P_{He} is the He production rate, t is the time for bubble evolution, and α, β are the constant depending on the bubble state. At the conditions of high temperature and/or low He production rate, the He bubble evolution will be the multi-atomic nucleation model which will follow the relationships as [35]:

$$C_B(t\to\infty) \sim 2C_B^* \propto \left(P_{He}/t^{\gamma} c_{Hel}^*\right)^{1/(\gamma+1)} \Big/ D_{Hel} \tag{5}$$

$$\overline{r_B}(t\to\infty) \propto \left[D_{Hel} c_{Hel}^{*\,1/(\gamma+1)} \left(P_{He}/t^{\gamma}\right)^{\gamma/(\gamma+1)} t^{\gamma+1}\right]^{1/\beta} \tag{6}$$

where c_{Hel}^* is the helium concentration in solution at nucleation peak, D_{Hel} is the He interstitial diffusion coefficient, γ is the constant. Till date, the two modes were successfully used to explain the He bubble formation at different irradiation scenarios, the He diffusivity has been regard as the controlling factor for He bubble evolution [32,36–38]. When we attempt to apply the models in our case, the criteria should be assessed in terms of their suitability. Theoretically, the transition from di-atomic nucleation to the multi-atomic nucleation will happen when the dissociation rate of a diatomic cluster becomes comparable with the rate of He absorption to it. And the "transition temperature" can increase with the He production rate [32]. In our situation, the irradiation temperatures located around the half-melting temperature regime while the He production rate by continuous implantation is up to ~2 appm/s in the peak region. So we suggest that the di-atomic nucleation would most likely happen when comparing to the previous studies performed in the similar conditions [32]. In our case, the He production rate and irradiation time are invariable, the formulas of (3a), (3b) can be further simplified as $C_B \propto (D_{He}^{eff})^{-3/7}$ and $\overline{r_B} \propto (D_{He}^{eff})^{1/7}$, when assuming $\alpha = 1$ (bulk diffusion controls the absorption of helium) [38], $\beta = 3$ (He bubble as non-ideal gas) [35]. They demonstrate a monotonic relationship between the He diffusivity and the He bubble behavior, that the increased He diffusivity at higher temperature is corresponding to the lower bubble number density and larger bubble size. It is consist with our observation for the temperature dependence of He bubble evolution. Moreover, a higher number density and smaller size observed in the HEA would imply its lower He diffusivity comparing to the Ni case, this speculation could also be verified by our aforementioned analysis on the He mobility in Ni and HEA. Therefore, we can conclude that the sluggish He diffusion effect in the HEA would have a prominent influence on the He bubble evolution, that nucleation was enhanced but growth was limited. For the underlying reason of He bubbles densely nucleated in the HEA, we inferred that the high lattice distortion in the HEA might be the one. It can induce the atomistic strain fields which acting as numerous physical sinks for bubble nucleation. In addition, the Table 2 indicates that the total volume of He bubbles formed in the HEA is less than that of Ni, and the difference is slightly larger at higher temperatures of 873 K and 973 K. The trend could also be explained by the featured energetics of point defects in the HEA. With increasing the irradiation temperature, the discrepancy of vacancy formation energy between Ni and HEA will amplify the effects of thermal vacancies on the He diffusion and bubble formation. Hence the less available thermal vacancies in the HEA will further suppress He bubble formation at a higher temperature.

Comparing to our previous investigation on the He bubble formation at the lower temperatures [24], the effect of sluggish He diffusion in the FeCoNiCr HEA seems to be evident until the temperature is high enough. It is because of the strong interaction between He and vacancies, which will alter the He migration mode from the SIA/He replacement mechanism to the vacancy dominated one as the temperature elevating to the half melting temperature. The "replacement mechanism" is an athermal process mainly controlled by the irradiation condition of damage rate [6], the unique intrinsic properties of HEA will not expect to have a substantial influence on the He diffusion behavior. However, when the temperature was moving to the regime of thermal vacancies highly activated, the He diffusion will be affected by the featured point defects behavior in the HEA.

5. Conclusion

In summary, the He bubble formation in the pure Ni and FeCoNiCr HEA were systematically investigated using the 2 MeV He^+ irradiation in the half-melting temperature regime. Our TEM observation found that the He bubble behaviors in both materials

have a typical temperature dependence, that larger bubble size and fewer number density showing in the higher temperature. At the same irradiation condition, stronger He bubble formation resistance display in the HEA because of its lower bubble volume fraction. For the behind reason, we suggest that the featured energetics of point defects in the HEA can enhance the recombination of defects and further lower the vacancy concentration during irradiation. As a consequence, He diffusion through the vacancy mechanism will be suppressed and it will further limit the bubble growth in the HEA.

Acknowledgment

This work was supported by Hong Kong Research Grant Council (RGC) [Grant No. CityU 11212915 and CityU 11205018], City University of Hong Kong [Grant No. CityU 9610425] and National Natural Science Foundation of China (NSFC) [Grant Nos. 11427904, and 11275005].

References

[1] I.E. Agency, World Energy Outlook 2018, 2018.
[2] S. Chu, A. Majumdar, Opportunities and challenges for a sustainable energy future, Nature 488 (7411) (2012) 294–303.
[3] U. DoE, A Technology Roadmap for Generation IV Nuclear Energy Systems, Nuclear Energy Research Advisory Committee and the Generation IV International Forum, 2002, pp. 48–52.
[4] S.J. Zinkle, G. Was, Materials challenges in nuclear energy, Acta Mater. 61 (3) (2013) 735–758.
[5] E.E. Bloom, S.J. Zinkle, F.W. Wiffen, Materials to deliver the promise of fusion power – progress and challenges, J. Nucl. Mater. 329–333 (2004) 12–19.
[6] H. Trinkaus, B.N. Singh, Helium accumulation in metals during irradiation – where do we stand? J. Nucl. Mater. 323 (2–3) (2003) 229–242.
[7] J.W. Yeh, S.K. Chen, S.J. Lin, J.Y. Gan, T.S. Chin, T.T. Shun, C.H. Tsau, S.Y. Chang, Nanostructured high-entropy alloys with multiple principal elements: novel alloy design concepts and outcomes, Adv. Eng. Mater. 6 (5) (2004) 299–303.
[8] Z. Li, K.G. Pradeep, Y. Deng, D. Raabe, C.C. Tasan, Metastable high-entropy dual-phase alloys overcome the strength–ductility trade-off, Nature 534 (7606) (2016) 227–230.
[9] B. Gludovatz, A. Hohenwarter, D. Catoor, E.H. Chang, E.P. George, R.O. Ritchie, A fracture-resistant high-entropy alloy for cryogenic applications, Science 345 (6201) (2014) 1153–1158.
[10] M.-H. Tsai, J.-W. Yeh, High-entropy alloys: a critical review, Mater. Res. Lett. 2 (3) (2014) 107–123.
[11] W. Kai, C.C. Li, F.P. Cheng, K.P. Chu, R.T. Huang, L.W. Tsay, J.J. Kai, The oxidation behavior of an equimolar FeCoNiCrMn high-entropy alloy at 950°C in various oxygen-containing atmospheres, Corros. Sci. 108 (Supplement C) (2016) 209–214.
[12] W. Kai, F.P. Cheng, C.Y. Liao, C.C. Li, R.T. Huang, J.J. Kai, The oxidation behavior of the quinary FeCoNiCrSix high-entropy alloys, Mater. Chem. Phys. 210 (2018) 362–369.
[13] S. Xia, M.C. Gao, T. Yang, P.K. Liaw, Y. Zhang, Phase stability and microstructures of high entropy alloys ion irradiated to high doses, J. Nucl. Mater. 480 (2016) 100–108.
[14] N.A.P.K. Kumar, C. Li, K.J. Leonard, H. Bei, S.J. Zinkle, Microstructural stability and mechanical behavior of FeNiMnCr high entropy alloy under ion irradiation, Acta Mater. 113 (2016) 230–244.
[15] C. Lu, T. Yang, K. Jin, N. Gao, P. Xiu, Y. Zhang, F. Gao, H. Bei, W.J. Weber, K. Sun, Y. Dong, L. Wang, Radiation-induced segregation on defect clusters in single-phase concentrated solid-solution alloys, Acta Mater. 127 (2017) 98–107.
[16] T. Yang, S. Xia, W. Guo, R. Hu, J.D. Poplawsky, G. Sha, Y. Fang, Z. Yan, C. Wang, C. Li, Y. Zhang, S.J. Zinkle, Y. Wang, Effects of temperature on the irradiation responses of Al0.1CoCrFeNi high entropy alloy, Scr. Mater. 144 (Supplement C) (2018) 31–35.
[17] Y. Zhang, G.M. Stocks, K. Jin, C. Lu, H. Bei, B.C. Sales, L. Wang, L.K. Béland, R.E. Stoller, G.D. Samolyuk, M. Caro, A. Caro, W.J. Weber, Influence of chemical disorder on energy dissipation and defect evolution in concentrated solid solution alloys, Nat. Commun. 6 (2015) 8736.
[18] T.-n. Yang, C. Lu, K. Jin, M.L. Crespillo, Y. Zhang, H. Bei, L. Wang, The effect of injected interstitials on void formation in self-ion irradiated nickel containing concentrated solid solution alloys, J. Nucl. Mater. 488 (2017) 328–337.
[19] T.-n. Yang, C. Lu, G. Velisa, K. Jin, P. Xiu, Y. Zhang, H. Bei, L. Wang, Influence of irradiation temperature on void swelling in NiCoFeCrMn and NiCoFeCrPd, Scr. Mater. 158 (2019) 57–61.
[20] Z. Fan, S. Zhao, K. Jin, D. Chen, Y.N. Osetskiy, Y. Wang, H. Bei, K.L. More, Y. Zhang, Helium irradiated cavity formation and defect energetics in Ni-based binary single-phase concentrated solid solution alloys, Acta Mater. 164 (2019) 283–292.
[21] D. Chen, Y. Tong, J. Wang, B. Han, Y.L. Zhao, F. He, J.J. Kai, Microstructural response of He + irradiated FeCoNiCrTi 0.2 high-entropy alloy, J. Nucl. Mater. 510 (2018) 187–192.
[22] S. Zhao, T. Egami, G.M. Stocks, Y. Zhang, Effect of d electrons on defect properties in equiatomic NiCoCr and NiCoFeCr concentrated solid solution alloys, Phys. Rev. Mater. 2 (1) (2018).
[23] S. Zhao, D. Chen, J.-J. Kai, First-principles study of He behavior in a NiCoFeCr concentrated solid–solution alloy, Mater. Res. Lett. 7 (5) (2019) 188–193.
[24] D. Chen, Y. Tong, H. Li, J. Wang, Y.L. Zhao, A. Hu, J.J. Kai, Helium accumulation and bubble formation in FeCoNiCr alloy under high fluence He+ implantation, J. Nucl. Mater. 501 (2018) 208–216.
[25] Z. Yan, S. Liu, S. Xia, Y. Zhang, Y. Wang, T. Yang, He behavior in Ni and Ni-based equiatomic solid solution alloy, J. Nucl. Mater. 505 (2018) 200–206.
[26] Z. Wu, H. Bei, F. Otto, G.M. Pharr, E.P. George, Recovery, recrystallization, grain growth and phase stability of a family of FCC-structured multi-component equiatomic solid solution alloys, Intermetallics 46 (2014) 131–140.
[27] H. Trinkaus, On the modeling of the high-temperature embrittlement of metals containing helium, J. Nucl. Mater. 118 (1) (1983) 39–49.
[28] J.F. Ziegler, M.D. Ziegler, J.P. Biersack, SRIM–The stopping and range of ions in matter (2010), Nucl. Instrum. Methods Phys. Res. Sect. B Beam Interact. Mater. Atoms 268 (11) (2010) 1818–1823.
[29] R.E. Stoller, M.B. Toloczko, G.S. Was, A.G. Certain, S. Dwaraknath, F.A. Garner, On the use of SRIM for computing radiation damage exposure, Nucl. Instrum. Methods Phys. Res. Sect. B Beam Interact. Mater. Atoms 310 (2013) 75–80.
[30] L.A. Giannuzzi, J.L. Drown, S.R. Brown, R.B. Irwin, F.A. Stevie, Applications of the FIB lift-out technique for TEM specimen preparation, Microsc. Res. Tech. 41 (4) (1998) 285–290.
[31] S.M. Allen, Foil thickness measurements from convergent-beam diffraction patterns, Philos. Mag. A 43 (2) (1981) 325–335.
[32] B. Singh, H. Trinkaus, An analysis of the bubble formation behaviour under different experimental conditions, J. Nucl. Mater. 186 (2) (1992) 153–165.
[33] G.S. Was, Fundamentals of Radiation Materials Science: Metals and Alloys, Springer, 2016.
[34] H. Trinkaus, Energetics and formation kinetics of helium bubbles in metals, Radiat. Eff. 78 (1–4) (2006) 189–211.
[35] H. Trinkaus, Modeling of helium effects in metals: high temperature embrittlement, J. Nucl. Mater. 133 (1985) 105–112.
[36] C. Zhang, K. Chen, Y. Wang, J. Sun, D. Shen, Formation of bubbles in helium implanted 316L stainless steel at temperatures between 25 and 550° C, J. Nucl. Mater. 245 (2–3) (1997) 210–216.
[37] Y.S. Wang, K.Q. Chen, C.H. Zhang, J.M. Quan, J.G. Sun, Z.Y. Zhao, The study of bubble formation in 316L stainless steel irradiated with helium ions at 873 K, J. Nucl. Mater. 240 (1) (1996) 70–74.
[38] V. Zell, H. Schroeder, H. Trinkaus, Helium bubble formation in nickel during hot implantation, J. Nucl. Mater. 212 (1994) 358–363.